IEEE Access
Multidisciplinary ⋮ Rapid Review ⋮ Open Access Journal

Received January 31, 2021, accepted February 6, 2021, date of publication February 10, 2021, date of current version February 19, 2021.

Digital Object Identifier 10.1109/ACCESS.2021.3058610

Marine Predators Algorithm Optimized Reduced Sensor Fuzzy-Logic Based Maximum Power Point Tracking of Fuel Cell-Battery Standalone Applications

MOKHTAR ALY[1,2], (Member, IEEE), EMAD M. AHMED[3,4], (Senior Member, IEEE), HEGAZY REZK[5,6], AND EMAD A. MOHAMED[1]

[1]Department of Electrical Engineering, Faculty of Engineering, Aswan University, Aswan 81542, Egypt
[2]Electronics Engineering Department, Universidad Tecnica Federico Santa Maria, Valparaiso 2390123, Chile
[3]Department of Electrical Engineering, College of Engineering, Jouf University, Sakaka 72388, Saudi Arabia
[4]AWCRC, Faculty of Engineering, Aswan University, Aswan 81542, Egypt
[5]College of Engineering at Wadi Addawaser, Prince Sattam Bin Abdulaziz University, Wadi Ad-Dawasir 11991, Saudi Arabia
[6]Electrical Engineering Department, Faculty of Engineering, Minia University, Minya 61517, Egypt

Corresponding author: Mokhtar Aly (mokhtar.aly@aswu.edu.eg)

This work was supported by the Deanship of Scientific Research, Prince Sattam Bin Abdulaziz University, through the Research Project, under Grant 2020/01/11742.

ABSTRACT Fuel cell (FC) represents one of the promising efficient solutions for future energy supply. Improving performance and integration methods of FCs via maximum power point tracking (MPPT) and high boosting factor inverters are key requirements for research in renewable energy fields. Recently, hybrid FC-battery structures have shown wide applications in several areas. Accordingly, marine predators algorithm (MPA) is proposed in this article for optimizing the design of reduced sensor fuzzy-logic based MPPT scheme. The proposed scheme inherits the following benefits: reduced sensors and hence reduced costs, more flexibility and smooth performance due to fuzzy-logic based MPPT, and optimized design method of fuzzy-logic based MPPT through MPA method. Moreover, a high boosting ratio inverter is introduced in this article based on using the switched capacitor multilevel inverter (SCMLI). The proposed system achieves self capacitor voltage control without complex control or extra sensors. The proposed hybrid FC-battery system has been validated at various operating points. In addition, comprehensive comparisons with existing schemes in the literature are provided in the paper. The superiority of the proposed scheme has been verified with robust, fast and accurate tracking, reduced cost, flexible, simple, and smooth output waveforms. The proposed method achieves the lowest output power fluctuations with fast tracking speed compared to the studied classical methods.

INDEX TERMS Battery, fuel cells (FCs), fuzzy logic control, marine predators algorithm, maximum power point tracking, stand alone applications.

I. INTRODUCTION

Energy represents the keystone driving factor for recent exhaustive economical worldwide developments through the reuse of available energy sources [1], [2]. Negative impacts resulting from fossil fuel-based electricity generation have induced research concerns for clean renewable generation sources [3]. The recent advancements and technology development of fuel cells (FCs) have lead to progressive increase in their employment [4]. FCs represent power generation components, which convert chemical potential to useful electrical energy. The different classifications of FCs are made based on the employed electrode type [5]. One promising kind of FCs is the proton exchange membrane FC (PEMFC) technology, which possesses improved efficiency [6]. Thence, PEMFCs have been preferred as energy supply alternatives. The main features of PEMFCs are their fast operation, the low operating temperatures, no resulting

The associate editor coordinating the review of this manuscript and approving it for publication was Sudhakar Babu Thanikanti.

contamination, and the higher power efficiencies [7]. However, nonlinearity exists in the output characteristics of PEMFCs and unique operating point exists for the maximum power point (MPP) operation [8].

Recently, MPP tracking (MPPT) schemes have been widely employed for solving the MPP uniqueness in several applications [8]. A single MPP exists for each combination of membrane water content and temperature in PEMFC applications [7]. Accordingly, MPPT controller has become an integral component of PEMFCs to continuously operate at their optimum output power. Several MPPT schemes have been presented for MPPT control for PEMFCs. The conventional perturb and observe (P&O) MPPT technique has been widely applied for PEMFC applications [9]. Additionally, the incremental resistance (IR) and incremental conductance (IC) have been widely selected for MPPT tracking with PEMFCs [10]–[12]. In [13], the PEMFC performance has been improved through the application of variable stepping size IR and IC schemes. Recently, meta-heuristic optimization and learning based schemes are presented for MPPT control in PEMFCs. In [14], the salp swarm optimizer (SSA) has been proposed for optimum determination for proportional integral derivative (PID) controller. Another tuning process for PID MPPT controller using the grey wolf optimization (GWO) scheme has been presented in [15]. Two different MPPT controllers have been introduced in [16] based on P&O and sine cosine optimization algorithm (SCA). Additionally, the ant-lion optimization algorithm (ALO) has been applied with PID control for off-grid FC applications [17]. In [18], the water cycle optimization algorithm has been proposed to determine the MPPT corresponding PEMFC voltage, which is tracked using cascaded PID controller. The dynamic cuckoo search optimization algorithm (DCSA) has been introduced for directly adjusting the duty cycle duration of boost DC/DC converter [19]. However, increased number of sensors is needed in the above-mentioned methods. The PEMFC current, and voltage measurements are required in these methods. Furthermore, some methods require additional temperature sensor for MPPT control.

Additionally, the neural network (NN) based on the radial basis function network (RBFN) has been proposed in [20]. In [21], artificial NN based on IC has been presented for enhancing the performance of PEMFCs. The ANFIS based MPPT technique has been introduced in [22]. The particle swarm optimizer based MPPT followed by PID controller has been introduced in [23]. Moreover, extremum seeking methods were employed in literature for determining the MPP position [24]. Another cascaded stage is added using PID controller for the tracking process. Fuzzy-logic control (FLC) based MPPT solutions have been applied in literature [25], [26]. The performance of MPPT control can be improved using proper design of FLC [27]. Hybrid IC-FLC method has been presented in [28]. FLC with optimized design was introduced in [29] for optimizing system response. The elitist invasive-weed optimizer (EIWO) has been utilized for optimum design of FLC in PEMFC applications [30]. The hybrid modified shuffled-frog leaping optimization algorithm (MSFLA) with FLC has been presented in [31]. Another hybrid BAT algorithm with FLC has been introduced in [32] for grid tied systems. The differential evaluation optimizer algorithms (DEOA) based FLC design was presented in [7] for PEMFC systems. The firefly optimized with asymmetrical FLC has been proposed in [33]. It can be seen from the previous literature review that existing schemes suffer from one or more of the following issues: increased number of required sensors, increased complexity, slow response, complicated implementation requirements, steady state fluctuations, and/or improper and inaccurate MPPT control.

From another side, PEMFCs face the issues of low output terminal voltage [34]. This in turn adds more requirements for the high boosting converters to integrate them with the AC loading. Several topologies have been introduced in literature for solving this issue. The boost DC/DC converter has been widely used for PEMFCs. Additionally, interleaved and multi-phase boost converters have been introduced for PEMFC applications [9], [35]. However, boost converters suffer from the low boosting factor of voltage. Another high step-up boost converter has been applied in [36] with PEMFC. The flyback converter has been proposed in [37] for FC applications. From another side, the boost DC/DC converter is used for the MPPT control between the PEMFC and battery side and it is followed by high gain DC/AC inverter stage. Among the various existing inverter topologies, the switched capacitor topologies have shown superior performance [38]–[40]. They eliminate the need for bulky inductor and magnetic components, and they achieve very high boosting factors, and simple control [41], [42]. Thence, a switched capacitor topology is presented in this article for hybrid PEMFC-battery standalone systems with high boosting gain.

Motivated by the above-mentioned issues and challenges in PEMFC stack systems, this article presents an optimized reduced sensor FLC (ORS-FLC) method for PEMFC applications. The optimized design of ORS-FLC method is achieved by the marine predators algorithm (MPA). The main contributions in this papers are:

- An optimized reduced-sensor FLC (ORS-FLC) MPPT scheme is proposed to achieve enhanced MPPT control for PEMFC stacks. The proposed ORS-FLC method employs only the output current sensors. The proposed method helps in reducing the cost of MPPT control. In addition, the optimized designs of FLC enables full utilization of fuzzy logic features.
- New applications for recent marine predators algorithm (MPA) is introduced in this article. The benefits of MPA is integrated with FLC features to provide enhanced MPPT control for PEMFC stack.
- A high boosting inverter is proposed in this article for elevating the low outputted voltage from PEMFC stack. The proposed inverter stage is based on switched capacitor cells with self balanced capacitor voltages.

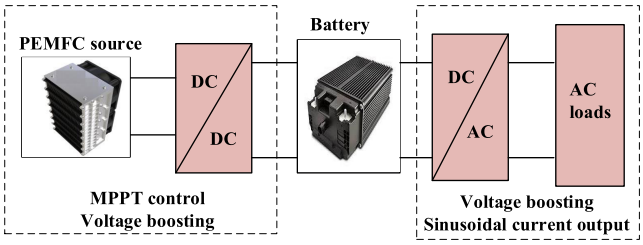

FIGURE 1. The structure and components of hybrid PEMFC-battery standalone system.

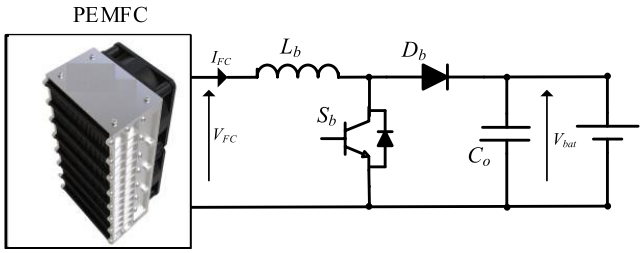

FIGURE 2. The circuit of PEMFC-side boost converter.

The proposed structure is advantageous for stepping up the low terminal voltage of PEMFCs to the load voltage levels.

- A reduced cost hybrid PEMFC-battery standalone system with low number of sensors, simple control, optimum design, and high boosting factor is proposed in this article.

The paper is organized as follows: Section II presents the hybrid PEMFC-battery stand alone system and its issues. Section III introduces the mathematical model and MPPT characteristics of PEMFCs. Section IV details the proposed ORS-FLC method for PEMFCs MPPT control. The optimization problem and methodology are provided in Section 5. The proposed high boosting inverter is explained in Section VI. Results and comparisons of proposed ORS-FLC method are provided in Section VII. Finally, the paper conclusion is shown in Section VIII.

II. PEMFC-BATTERY STANDALONE SYSTEM

Fig. 1 shows the structure for the standalone PEMFC-battery system. The output of PEMFC is fed to the battery side through DC/DC power conversion circuit. Then, the battery side is responsible for supplying electrical power to the AC load side. There are different functionalities that are required from the various components. The DC/DC power conversion circuit is responsible for boosting the output of PEMFC to suitable level for the battery. The outputted terminal voltage from the PEMFC is low and hence step-up circuit is required. Moreover, it is required to operate the PEMFC at high efficiency. In addition, the battery has to raise its terminal voltage to suitable level for the AC load or grid side integration.

The boost converter is selected for the DC/DC power conversion side. It is also responsible for the MPPT control for the PEMFC at various operating conditions. The duty cycle of boost converter is controlled so as to preserve the MPPT operation. There are a unique operating point for MPPT at each operating combination. A continuous tracking is essential for maximizing the system efficiency. In PEMFC applications, the temperature and membrane water content are the most influencing parameters for the MPP. The power circuit for the PEMFC side boost converter is shown in Fig. 2. The main functions of this converter are the continuous tracking for system MPPT, and the boosting of low voltage level at PEMFC terminals to suitable higher voltage for the battery terminal. The MPPT algorithm is responsible for the determination of duty cycle operation for the boost converter based on the measured signals. In this article, a reduced sensor MPPT algorithm is proposed compared to the higher number of sensors in existing methods. The input voltage of boost converter at PEMFC side V_{FC} is related to the output voltage at battery side V_{bat} and the duty cycle D as follows:

$$\frac{V_{\mathrm{bat}}}{V_{\mathrm{FC}}} = \frac{1}{1-D} \tag{1}$$

From another side, batteries have lower voltages than the load side. A very high boosting factor DC/AC power conversion stage is needed. In the proposed system, the boost converter is selected for the PEMFC side, which results in very low voltages of the employed battery side. Thence, a very high boost inverter stage is used in battery-load side. There are several requirements at the DC/AC inverter stage, including the high boosting factor, sinusoidal output current injection, active and reactive power control/supply, and low total harmonic distortion (THD) in outputted voltage/current waveforms. Usually pulse width modulation (PWM) is needed for operating the inverter stage. In the following sections, the principle and PWM generation of the proposed high boosting factor inverter stage are given in details.

III. PEMFC MODELLING

A. MATHEMATICAL MODEL

The performance of PEMFC is dependant on different factors, including the membrane water content in addition to operating temperature. The various elements of PEMFC can be represented as following:

1) TERMINAL VOLTAGE MODELLING

PEMFCs inherit different components that affects their output. The output terminal voltage V_{FC} of PEMFC stack can be expressed as follows:

$$V_{\mathrm{FC}} = N_{\mathrm{FC}} \times V_{\mathrm{cell}} = N_{\mathrm{FC}} \times (E_{\mathrm{Nernest}} - V_{\mathrm{act}} - V_{\mathrm{ohm}} - V_{\mathrm{con}}) \tag{2}$$

where, N_{FC} denotes to numbers of cells in PEMFC stack, V_{cell} output terminal voltage of PEMFC stack, E_{Nernest} denotes to the component of Nernest voltage, V_{act} is the activation component, V_{con} is the concentration loss component, and V_{ohm} represents the ohmic component. The total outputted

power from PEMFC stack P_{FC} is modelled as following:

$$P_{FC} = V_{FC} I_{FC} \tag{3}$$

2) $E_{Nernest}$ MODELLING

The component of $E_{Nernest}$ can be expressed as follows:

$$E_{Nernest} = 1.229 - 8.5 \times 10^{-4}(T - 298.15) + 4.385 \times 10^{-5} T(\ln P_{H_2} + 0.5 \ln P_{O_2}), \tag{4}$$

3) V_{act} MODELLING

The component of V_{act} is expressed as following [23]:

$$V_{act} = -[\xi_1 + \xi_2 T + \xi_3 T \ln(C_{O_2}) + \xi_4 T \ln(I_{FC})] \tag{5}$$

where, ξ_1, ξ_2, ξ_3, ξ_4 represent parametric coefficients for PEMFCs, which are extracted through fitting of experimental results and using recent optimization methods [14], [23]. The concentration of the dissolved oxygen C_{O_2} for the gas-liquid interface, which is modelled as follows:

$$C_{O_2} = \frac{P_{O_2}}{(5.08 \times 10^6) \times \exp(-498/T)} \tag{6}$$

4) V_{ohm} MODELLING

The V_{ohm} component is dissipated through the membrane ohmic resistance. It is expressed as follows:

$$V_{ohm} = I_{FC} \frac{r_m l}{A} \tag{7}$$

where, r_m denotes to the membrane resistivity to the conductivity of proton, l denotes to membrane thickness, and A is the active area of PEMFC. The resistivity r_m depends mainly on the humidity and the temperature of membrane. It is expressed as follows [10]:

$$r_m = \frac{181.8[1 + 0.03(\frac{I_{FC}}{A}) + 0.0062(\frac{T}{303})(\frac{I_{FC}}{A})^{2.5})]}{[\lambda_m - 0.634 - 3(\frac{I_{FC}}{A}) \exp(4.18\frac{T-303}{T})]} \tag{8}$$

where, λ_m is the membrane water content.

5) V_{con} MODELLING

The component of V_{con} results from consumption of the concentration gradients for the reactants. It is expressed as follows:

$$V_{con} = \frac{RT}{nF} \ln(1 - \frac{I_{FC}}{I_{max} A}) \tag{9}$$

where, n is the number for participated electrons in the reaction process, and I_{max} is the peak limiting current.

B. MPPT UNIQUENESS

The previous models are combined to provide modelling for PEMFC stack. The Matlab program has been used for the model based on the selected PEMFC specifications from [7]. Table 1 summarizes the specifications of the modelled PEMFC stack in the proposed scheme. The modelled PEMFC stack is validated for different membrane water content λ_m and temperature T. The obtained P_{FC}-I_{FC} at various operating λ_m and constant T of 303 K are shown in Fig. 3a. Whereas, the obtained P_{FC}-I_{FC} at various operating T and constant λ_m of 10 are shown in Fig. 3b. It can be seen from Fig. 3 the uniqueness of MPPT of PEMFC stack. The stack has to be continuously operated at the point, which corresponds to MPPT location. The nonlinearity of PEMFC output characteristics exhibits a unique MPPT for each combination of λ_m and T. Therefore, MPPT controller has become essential part for more efficient operation of PEMFC stacks.

TABLE 1. The parameters of the selected PEMFC stack [7].

Parameters	Values
T	303-363 (K)
λ_m	10-16
A	232 (cm^2)
N_{FC}	35
l	0.0178 (cm)
n	2
I_{max}	2.00 (A cm^{-2})
F	96484600 (C $(kmol^{-1})$
$q^{in}_{O_2}$	5×10^{-5} (kmol $(S)^{-1}$)
R	8.31447 (J (mol $K)^{-1}$)
k_{O_2}	2.11×10^{-5} (kmol (atom $S)^{-1}$)
k_r	9.07×10^{-8} (J (mol $K)^{-1}$)
$q^{in}_{H_2}$	10×10^{-5} (kmol $(S)^{-1}$)
k_{H_2}	4.22×10^{-5} (kmol (atom $S)^{-1}$)
ξ_1	0.944
ξ_2	0.00354
ξ_3	7.8×10^{-8}
ξ_4	-1.96×10^{-4}

IV. THE PROPOSED ORS-FLC MPPT SCHEME

A. TRADITIONAL FLC-BASED MPPT

The traditional used criteria for locating the position of MPP is through employing the slope (dP_{FC}/dV_{FC}). In these methods, two inputs are usually employed as inputs for the FLC method, namely the error E and change in error ΔE. They can be represented as follows:

$$E(k) = \frac{dP_{FC}}{dV_{FC}} = \frac{P_{FC}(k) - P_{FC}(k-1)}{V_{FC}(k) - V_{FC}(k-1)} \tag{10}$$

$$\Delta E(k) = E(k) - E(k-1) \tag{11}$$

where, $E(k)$, $E(k-1)$, and $\Delta E(k)$ are the estimated error at (k) sample, the error at $(k-1)$ sample, and the change in error at (k) sample, respectively. However, this method requires sensing both of the terminal voltage and output current from PEMFC.

B. PROPOSED ORS-FLC MPPT METHOD

In the proposed method, it is aimed to develop a new optimized FLC scheme with reduced number of sensors, particularly through using the current measurement only and eliminating the voltage measurement from the PEMFC terminals. The output power from the PEMFC can be represented as follows:

$$P_{FC} = V_{FC} I_{FC} \tag{12}$$

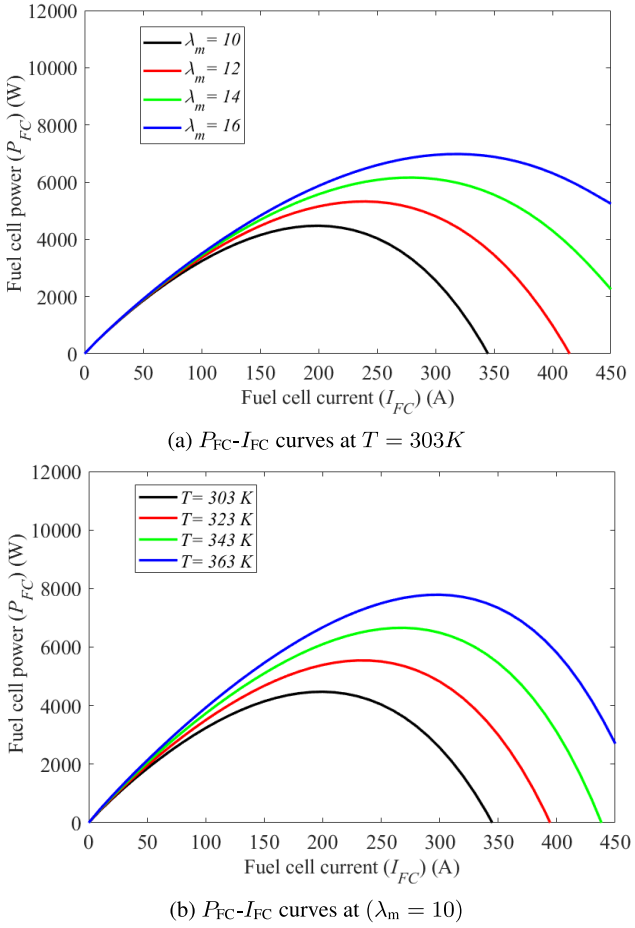

(a) P_{FC}-I_{FC} curves at $T = 303K$

(b) P_{FC}-I_{FC} curves at ($\lambda_m = 10$)

FIGURE 3. The characterstics P_{FC}-I_{FC} of PEMFC stack.

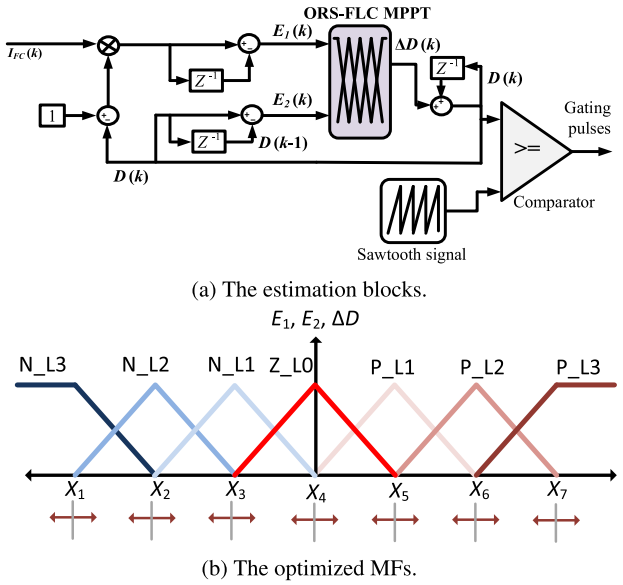

(a) The estimation blocks.

(b) The optimized MFs.

FIGURE 4. The estimations block and the optimized MF shape for the proposed ORS-FLC scheme.

By using the relation between V_{FC} and V_{bat} from (1), then (12) can be expressed as following:

$$P_{FC} = V_{bat}(1 - D)I_{FC} \tag{13}$$

It can be seen from (13) that the PEMFC power is related to the battery voltage, the boost duty cycle, and the PEMFC current. The battery voltage can be assumed constant due to the low variations of the battery voltage. Whereas, the boost duty cycle is already available inside the controller. Then, the PEMFC output power can be estimated by only sensing the PEMFC current.

In the proposed ORS-FLC MPPT method, there are two inputs are utilized for the FLC algorithm. The first input E_1 can be expressed as following:

$$\begin{aligned} E_1(k) &= P_1(k) - P_1(k-1) \\ &= [I_{FC}(k) \times (1 - D(k))] - P_1(k-1) \end{aligned} \tag{14}$$

And, the second input E_2 can be represented as following:

$$E_2(k) = D(k) - D(k-1) \tag{15}$$

Fig. 4a shows the block diagram representation for the estimations of the two inputs E_1 and E_2. It can be seen that the proposed ORS-FLC method employs a single sensor for MPPT tracking. Thence, reduced cost of the PEMFC system can be achieved using the proposed method. Afterwards, the estimated signals E_1 and E_2 are fed into the FLC method so as to generate the controlling duty cycle for the boost converter at the MPP corresponding position.

The FLC-based MPPT control is usually composed of three major phases, including the fuzzification phase, fuzzy-rules evaluation phase, and the defuzzification phase. Throughout the fuzzification phase, the two inputs are evaluated based on the utilized membership functions (MFs). The physical signals are transformed into suitable inputs for FLC systems. These evaluations are performed using the selected triangular MFs for both the two inputs in the proposed method. In the fuzzy-rules evaluation phase, the fed estimations from fuzzification stage are evaluated according to the fuzzy rules set. Table 2 shows the fuzzy rules in the proposed ORS-FLC method. Each of the two inputs and the output are represented by total of 7 different levels as follows: three for positive level side, P_L3, P_L2, P_L1, zero level Z_L0, and three negative levels N_L3, N_L2, N_L1. Thence, total of 49 rules exist in the proposed ORS-FLC MPPT method. The employed number of levels in each MF helps in smoothing the output waveforms of the PEMFC during transient and steady state conditions. The high number of levels does not impose restrictions on the implementation of the proposed method due to the suitability of FLC for low cost implementation. Lastly, defuzzification phase functions to determine the suitable output duty cycle for boost converter using the evaluated fuzzy rules. The change of boost duty cycle is generated in this phase until the MPP is reached. The defuzzification phase is expressed as follows:

$$\Delta D(k) = \frac{\sum_{i=1}^{49} W_i C_j}{\sum_{i=1}^{49} W_i} \tag{16}$$

TABLE 2. The fuzzy rules in the proposed ORS-FLC MPPT methodology.

Input MFs		E_2						
		N_L3	N_L2	N_L1	Z_L0	P_L1	P_L2	P_L3
E_1	N_L3	N_L3	N_L3	N_L3	Z_L0	P_L1	P_L2	P_L3
	N_L2	N_L3	N_L2	N_L2	Z_L0	P_L1	P_L2	P_L3
	N_L1	N_L2	N_L2	N_L1	Z_L0	P_L1	P_L1	P_L2
	Z_L0	Z_L0	Z_L0	Z_L0	Z_L0	Z_L0	Z_L0	Z_L0
	P_L1	P_L2	P_L2	P_L1	Z_L0	N_L1	N_L1	N_L2
	P_L2	P_L3	P_L2	P_L2	Z_L0	N_L2	N_L2	N_L3
	P_L3	P_L3	P_L3	P_L3	Z_L0	N_L3	N_L3	N_L3

where, $W_{\rm i}$ denotes to minimum MF number for the $i^{\rm th}$ rule, and $C_{\rm j}$ represents center value for FLC MF output. After the generation of FLC outputted ΔD, the current sampling instant duty cycle is generated, and the compared to saw-tooth signal with fixed switching frequency to generate the control gating pulses for the boost converter.

C. OPTIMIZING THE FLC SYSTEM

The behavior of FLC systems is basically determined by the designed MFs of inputs and outputs. In the proposed design methodology, an optimized design and determination methods are proposed for the MFs of both inputs and outputs in the FLC MPPT controller. The main objectives for the design methodology are the accurate and fast tracking for MPP location. Fig. 4b shows the principle for the MF optimized design for inputs E_1 and E_2 and output ΔD. The proposed ORS-FLC method is designed through optimal determination for the various points in the MFs. This can be achieved through proper tuning for the inner and outer points of the MFs. In the classical designs, only the outer points are determined while keeping fixed distances among internal point within the interval. Instead, the proposed ORS-FLC method employs the MPA optimizer to determine optimum location of each point in the MF shape. In the following section, the objective function and optimization process are given in details.

V. OPTIMIZATION METHODOLOGY

A. MPA OPTIMIZER

The principle for MPA inspiration can be represented by widespread searching for food strategy that is the movements of Levy in addition to Brownie in the surrounding predators along with an optimal encounter for modified policy within the biological interaction between predators and preys. More details regarding the core idea in addition to mathematical representations can be found in [43]. The MPA optimizer takes the advantage of good memory in reminding of their associates as well as the location of successful foraging. The procedures of MPA include three phases based on the speed ratio among preys in addition to predators. They can be explained as follows:

Phase 1 (High-Speed Ratio): In this phase, it is assumed that the prey is faster than predator. Such a stage is carried out during the first third of iterations. The prey follows the next relation to modify its location. It can be expressed as follows:

$$S_{\rm i} = R_{\rm B} \times (Elite_{\rm i} - R_{\rm B} \times Z_{\rm i}), i = 1, 2, \ldots, n \quad (17)$$

$$Z_{\rm i} = Z_{\rm i} + P.R \times S_{\rm i} \quad (18)$$

where, $R \in [\,0, 1\,]$ is a vector of random numbers, $P = 0.5$ and R_B is Brownian motion vector.

Phase 2 (Unity Speed Ratio): Both speed values of prey and predator velocity are assumed to be identical during this stage. This stage is carried out in the middle of the process. The predator moves according to Brownian approach, whereas the prey moves according to Lévy flight approach. The population is divided into two subsections; the first section employs (19) and (20), whereas the other section uses (21) and (22) to modify the locations as follows:

$$S_{\rm i} = R_{\rm L} \times (Elite_{\rm i} - R_{\rm L} \times Z_{\rm i}), i = 1, 2, \ldots, n/2 \quad (19)$$

$$Z_{\rm i} = Z_{\rm i} + P.R \times S_{\rm i} \quad (20)$$

where R_L is a variable generated randomly by Lévy distribution.

$$S_{\rm i} = R_{\rm B} \times (R_{\rm B} \times Elite_{\rm i} - Z_{\rm i}), i = 1, 2, \ldots, n/2 \quad (21)$$

$$Z_{\rm i} = Elite_{\rm i} + P.CF \times S_{\rm i} \quad (22)$$

where,

$$CF = (1 - \frac{t}{t_{\max}})^{2\frac{t}{t_{\max}}} \quad (23)$$

where t and $t_{\max}$ are the current and max number of iterations.

Phase 3 (Low-Speed Ratio): On the contrary with the first stage, the speed of predator is greater than prey in the third stage. This stage is carried out in the last third of iterations. The location is modified based on the next relation:

$$S_{\rm i} = R_{\rm L} \times (R_{\rm L} \times Elite_{\rm i} - Z_{\rm i}), i = 1, 2, \ldots, n \quad (24)$$

$$Z_{\rm i} = Elite_{\rm i} + P.CF \times S_{\rm i}, CF = (1 - \frac{t}{t_{\max}})^{2\frac{t}{t_{\max}}} \quad (25)$$

B. OBJECTIVE FUNCTION

The various phases of the FLC have been programmed in Matlab/m-file so as to provide flexible platform for the optimizer to determine the optimum design points. Fig. 5 shows the structure of the proposed optimization procedures. The inputs for the FLC E_1 and E_2 are firstly estimated based on (14), and (15), respectively. The proposed MPA optimizer targets to determine the optimum values for the various points of the ORS-FLC method for both the inputs and

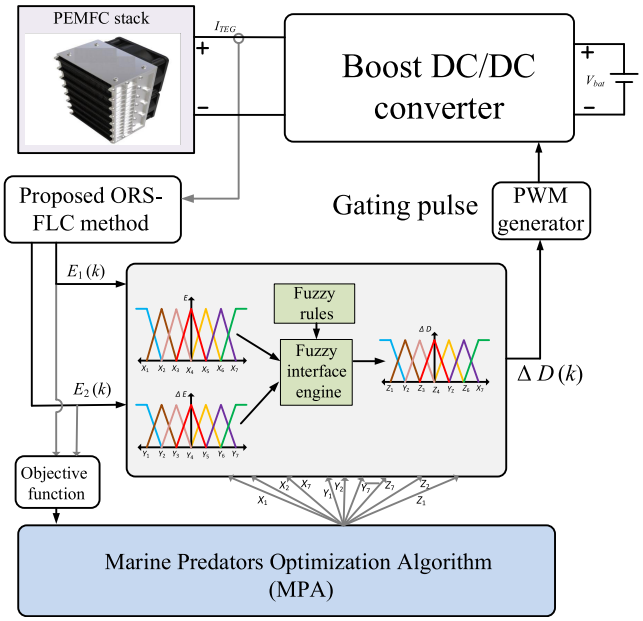

FIGURE 5. The block diagram representation for the MPA-based optimization of the proposed ORS-FLC method.

output MFs. When the selected objective function becomes optimum, the iterations are completed and the designed values of the points are outputted. The proposed method adds more flexibility through optimizing the inner and outer points of MFs. The objective function in the proposed ORS-FLC method is designed based on integral absolute-error (IAE) criteria for the slope (dP_{FC}/dV_{FC}) as preferred criteria for MPPT position. The objective function can be modelled as following:

$$IAE = \int_{t=o}^{T_{sim}} abs(\frac{dP_{FC}}{dV_{FC}}).dt = \int_{t=o}^{T_{sim}} abs(\frac{P_{FC}(k) - P_{FC}(k-1)}{V_{FC}(k) - V_{FC}(k-1)}).dt \quad (26)$$

where, T_{sim} is the time of simulation process for the evaluations of the IAE objective function. The optimizer locates the various combination of design points of inputs and output MFs simultaneously.

VI. THE PROPOSED DC/AC INVERTER STAGE

Since the battery voltage is very low, the conventional voltage source converters (VSC) or current source inverters (CSI) cannot be used to convert the low battery voltage to the required AC load voltage (110 V_{rms}). Therefore, a high boosting DC-AC inverter stage is required. Several topologies are addressed in the literature that have high boosting ratio [38], [39], wherein multilevel inverters (MLIs) have gained high interests due to their high efficiency, high power density, modularity and decreased voltage stresses across the semiconductor switches. A switched capacitor MLI (SCMLI) is selected for our case study [40]. Fig. 6 shows the 9-levels SCMLI topology based on the switched capacitors structure. This converter is developed using a single DC source (battery) and a repeated cell contains a capacitor combined with 5-power switches. This topology is capable of achieving 4 timed boosting factor for the battery voltage. The inverter output can be expressed as follows:

$$V_{AC,load} = 4V_{bat} \times mi \times sin(\omega t) \quad (27)$$

where, mi represents the modulation index of the modulating signal, and $V_{AC,load}$ denotes to the peak output AC voltage. Therefore, by combining the boost converter boosting with the inverter boosting, (27) can be expressed as follows:

$$V_{AC,load} = \frac{4V_{FC}}{1-D} \times mi \times sin(\omega t) \quad (28)$$

It is worth mentioning that all the semiconductor switches in this topology have the same voltage stresses and it equals to the battery voltage. Furthermore, all the capacitors are inherently self-balanced since all the capacitors are connected in parallel every line cycle to be charged equally from the battery. The operation of such inverter is quite simple as in the beginning of each line cycle, all the capacitors are charged to have the same battery voltage as all the semiconductor switches S_4, S_6, S_8, S_9, S_{14}, S_{11}, S_{13}, S_{16}, S_{18}, S_{19} are switched ON while the output voltage equals to zero state. However, for generating the output voltage with the required magnitude and frequency, a carrier based pulse width modulation (PWM) is used, wherein a 50 Hz modulated sinusoidal voltage signal is compared with 8-level shifted carrier signals with switching frequency equals to 30 kHz. The switching table for producing the required output voltage levels is shown in Table 3.

VII. RESULTS AND PERFORMANCE VERIFICATION

The aforementioned parameters for the modelled PMFC stack in Table. 1 have been built in Matlab with the proposed ORS-FLC MPPT method. Moreover, the widely used P&O and classical FLC methods have been implemented for comparison purposes with the new proposed method. The parameters for boost power conversion stage includes inductance L_b of 500 μH, output capacitance C_o of 500 μF, saw-tooth signal frequency of 10 kHz, and the battery has 50 V nominal voltage. The proposed ORS-FLC MPPT method has been validated at the initial transients, step changes in λ_m with constant values of T, and step changes in T with constant values of λ_m.

Fig. 7 shows the performance comparisons between the proposed ORS-FLC MPPT method with classical FLC and P&O method at initial starting case with λ_m equals to 13 and T equals to 343 k. The behavior of extracted power output under the three methods is shown in Fig. 7a. It can be seen that the proposed ORS-FLC method has smooth and fast tracking for the power output. The proposed method exhibits fast settling time for MPPT. Moreover, higher tracking accuracy can be obtained in addition to low fluctuated power during initial transients by using the proposed ORS-FLC method. The proposed method achieves the minimum output

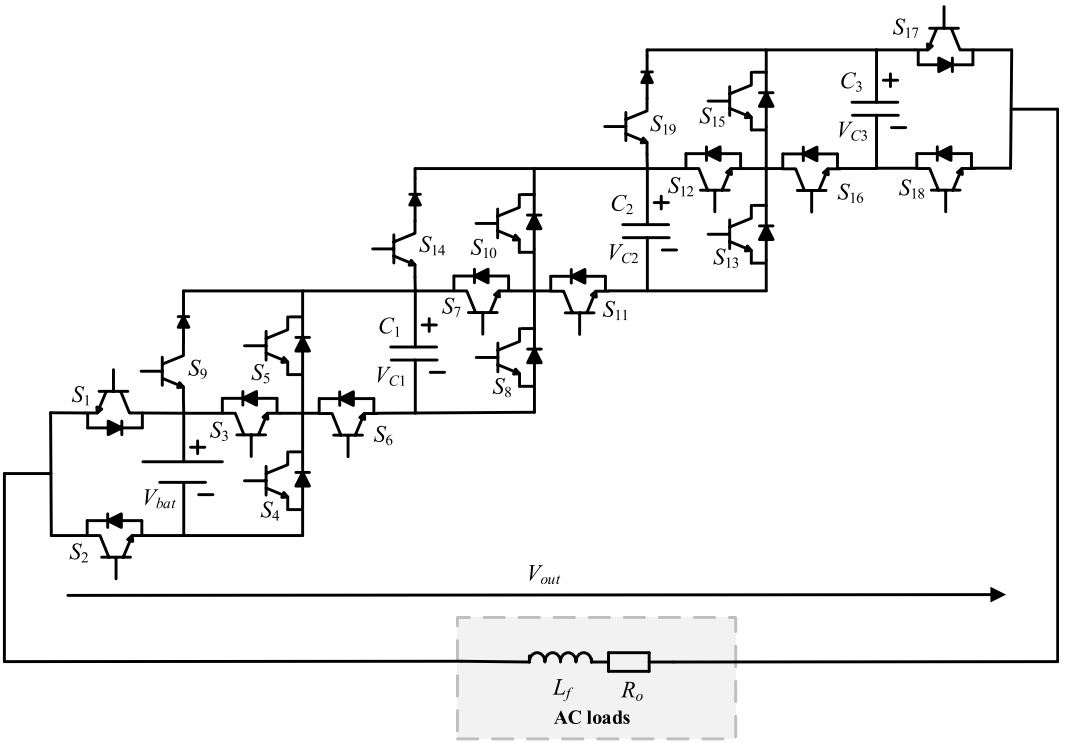

FIGURE 6. The power circuit of the step-up inverter.

TABLE 3. Switching states of the high boosting inverter topology (1 for ON and 0 for OFF).

Output	Switch Signals																		
	S_1	S_2	S_3	S_4	S_5	S_6	S_7	S_8	S_9	S_{10}	S_{11}	S_{12}	S_{13}	S_{14}	S_{15}	S_{16}	S_{17}	S_{18}	S_{19}
$4\,V_{dc}$	1	0	0	1	1	0	0	1	0	1	0	0	1	0	1	0	0	1	0
$3\,V_{dc}$	1	0	0	1	1	0	0	1	0	1	0	0	1	0	0	1	0	1	0
$2\,V_{dc}$	1	0	0	1	1	0	0	1	0	0	1	0	1	0	0	1	0	1	0
V_{dc}	1	0	0	1	0	1	0	1	0	0	1	0	1	0	0	1	0	1	0
0	0	1	0	1	0	1	0	1	1	0	1	0	1	1	0	1	0	1	1
$-V_{dc}$	0	1	1	0	0	1	0	1	0	0	1	0	1	0	0	1	0	1	0
$-2V_{dc}$	0	1	1	0	0	1	1	0	0	0	1	0	1	0	0	1	0	1	0
$-3V_{dc}$	0	1	1	0	0	1	1	0	0	0	1	1	0	0	0	1	0	1	0
$-4V_{dc}$	0	1	1	0	0	1	1	0	0	0	1	1	0	0	0	1	1	0	0

power fluctuations compared with the classical FLC and P&O methods. Additionally, the performance of voltage output under the three methods is shown in Fig. 7b. The proposed method achieves fast tracking of MPPT without high overshoot/undershoot spikes in the output voltage. In addition, reduced fluctuations are obtained using the proposed method compared to classical FLC and P&O methods. Whereas, the performance of current output from PEMFC under the three methods is shown in Fig. 7c. It can be seen that classical FLC and P&O methods have high overshoot spikes in the output current at the starting. The high spikes deteriorate the lifetime of PEMFC and other electrical components. Instead, the proposed ORS-FLC MPPT method does not have overshoot spikes, and hence reduced stresses are obtained over the PEMFC and other components.

Fig. 8 shows the performance of the three methods with step changes in λ_m by reduction from 13 to 10 with constant T of 343 K at time 0.15s. The performance of power extraction is compared in Fig. 8a. The lowest oscillations are achieved by the proposed ORS-FLC MPPT method, whereas the classical FLC and P&O methods have high oscillations at steady state. In addition, smooth tracking of MPP is achieved with the proposed ORS-FLC method. The comparison of output voltages is shown in Fig. 8b. The P&O method possesses the highest spike in the terminal voltage of PEMFC. The high spikes add more stresses on the PEMFC and hence reduced lifetime. The classical FLC has improved response from P&O method. The proposed method mitigates the spikes of PEMFC voltage waveform. Fig. 8c compares the output current of the three considered methods. The undershoot spikes become clear in the response of P&O method followed by classical FLC method. It can be seen from the response of the proposed method that it has reduced current spike with mitigated steady state fluctuations.

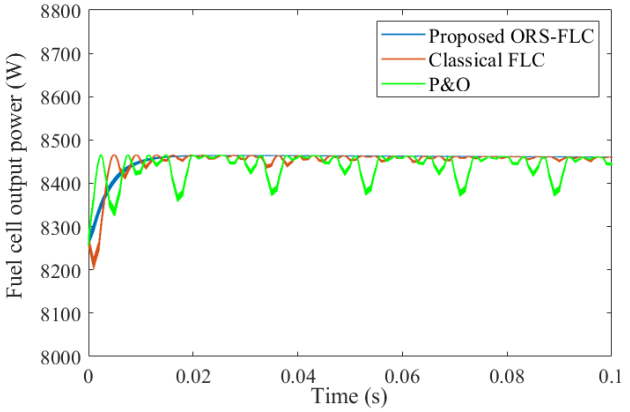

(a) The PEMFC output power.

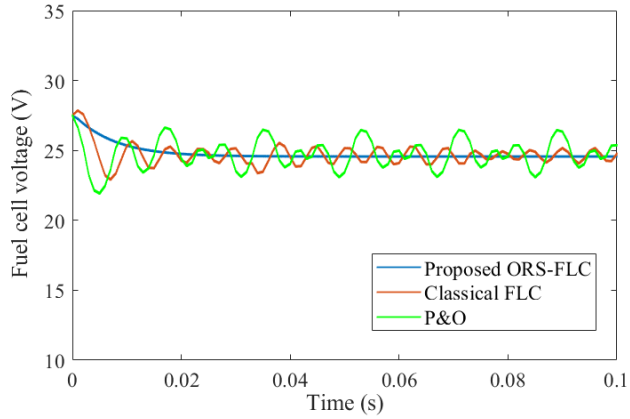

(b) The PEMFC output voltage.

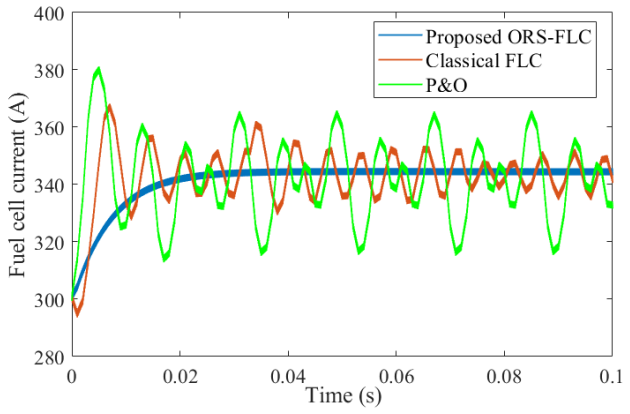

(c) The PEMFC output current.

FIGURE 7. Performance comparison of the proposed ORS-FLC scheme at transient start.

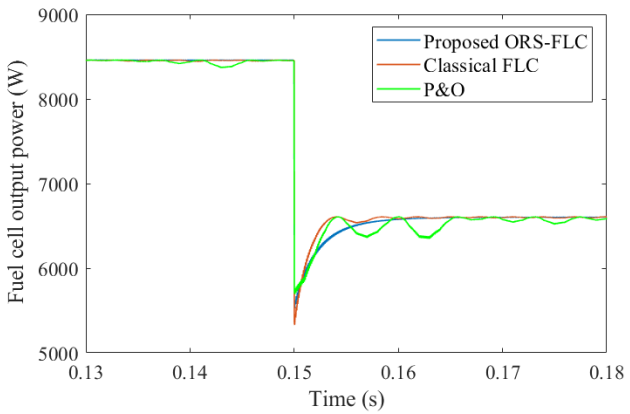

(a) The PEMFC output power.

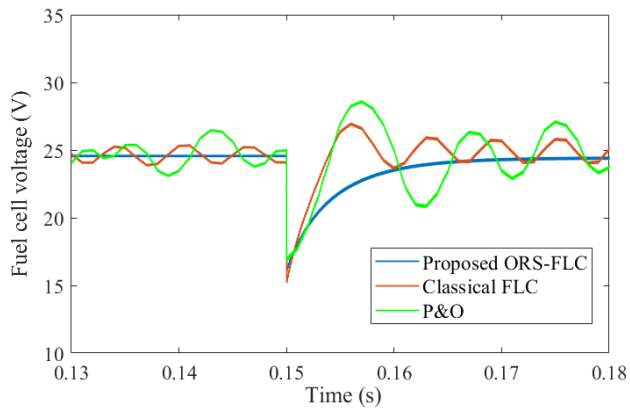

(b) The PEMFC output voltage.

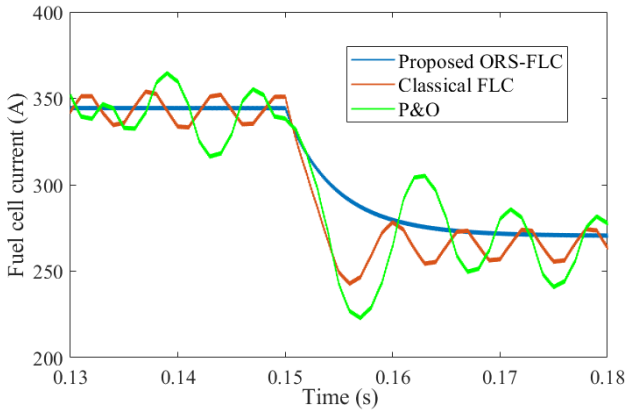

(c) The PEMFC output current.

FIGURE 8. Performance comparison of the proposed ORS-FLC scheme at step decrease in λ_m.

Fig. 9 shows the performance of the three methods at step changes in λ_m at increase from 10 to 13 with constant T of 343 K at time 0.25s. It can be seen from the outputted maximum power in Fig. 9a that the proposed method has improved transient and steady state oscillations. The proposed ORS-FLC method extracts efficiently the MPP at various operating conditions. Moreover, the proposed method can effectively eliminate the steady state oscillations in the extracted MPP from PEMFCs. In contrast, the classical FLC and P&O methods possess increased oscillations during transient and steady state waveforms. The P&O method has the highest output power fluctuation, whereas the proposed method has the minimum power fluctuations. The terminal voltages of the three cases are compared in Fig. 9b. The oscillated response of P&O in addition to classical FLC methods have become clear compared to the mitigated oscillations of the proposed ORS-FLC MPPT method. Moreover, the P&O method has the highest current overshoot value as shown

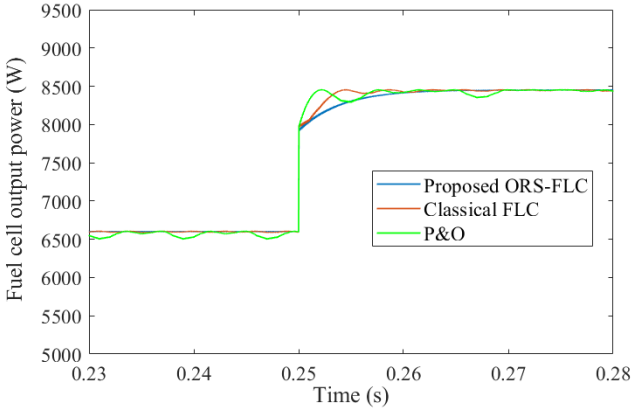

(a) The PEMFC output power.

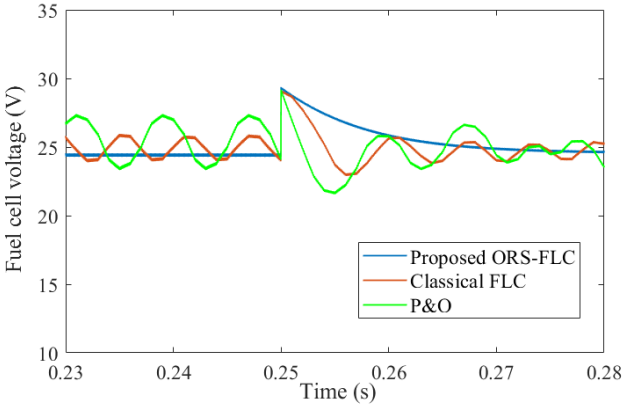

(b) The PEMFC output voltage.

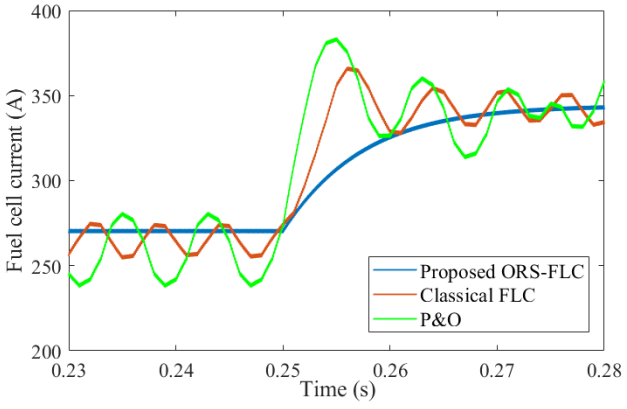

(c) The PEMFC output current.

FIGURE 9. Performance comparison of the proposed ORS-FLC scheme at step increase in λ_m.

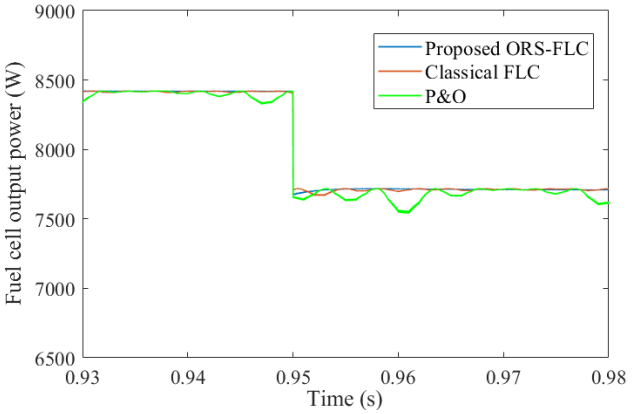

(a) The PEMFC output power.

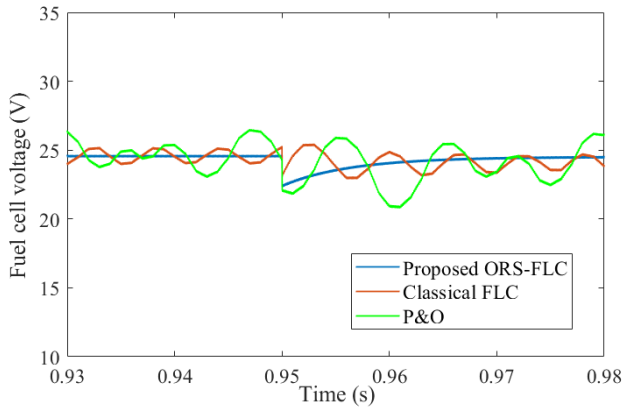

(b) The PEMFC output voltage.

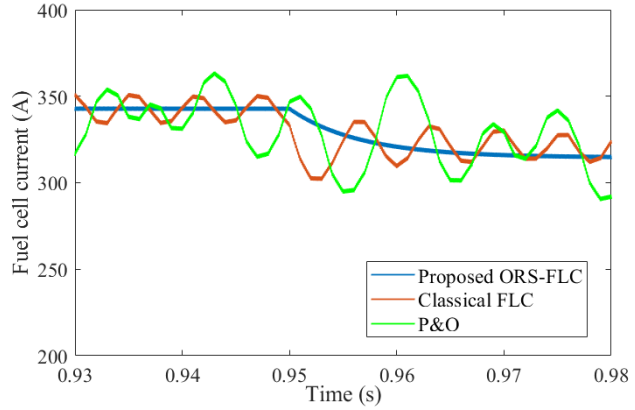

(c) The PEMFC output current.

FIGURE 10. Performance comparison of the proposed ORS-FLC scheme at step decrease in T.

in Fig. 9c. The same increased overshoot happens with applying classical FLC method. The proposed method is successful at eliminating the overshoot spikes in the outputted current of PEMFC at λ_m step changes.

In this case, the three methods are compared at step change reduction in T from 343 K to 333 K at time 0.95s and constant λ_m of 13 as shown in Fig. 10. The comparison of extracted power waveforms is shows in Fig. 10a. It has become obvious that the proposed ORS-FLC method tracks the MPP at both operating points with fast transient and reduced power ripples at steady state. The worst response is obtained by the P&O method due to the high power oscillations in steady state. The terminal voltage and current waveforms are shown in Fig. 10b and Fig. 10c, respectively. The highest oscillations exist in the P&O method followed by the classical FLC method. The two methods have high ripples in steady state waveforms of outputted voltage and current. Apart from that, the proposed ORS-FLC method possesses mitigated oscillation in both the terminal voltage and current from PEMFC stack.

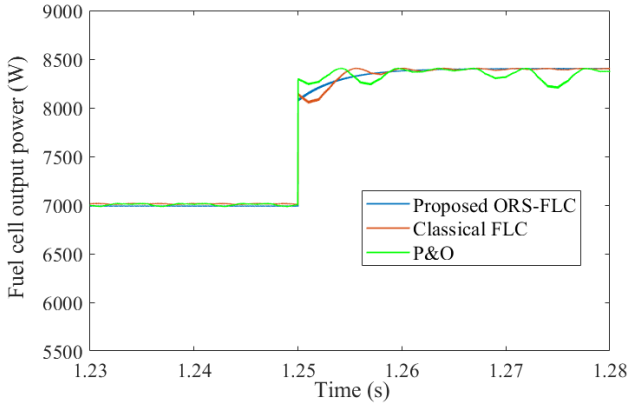

(a) The PEMFC outputted power.

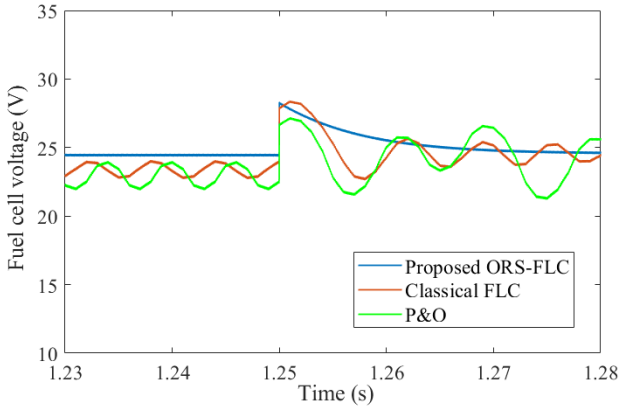

(b) The PEMFC output voltage.

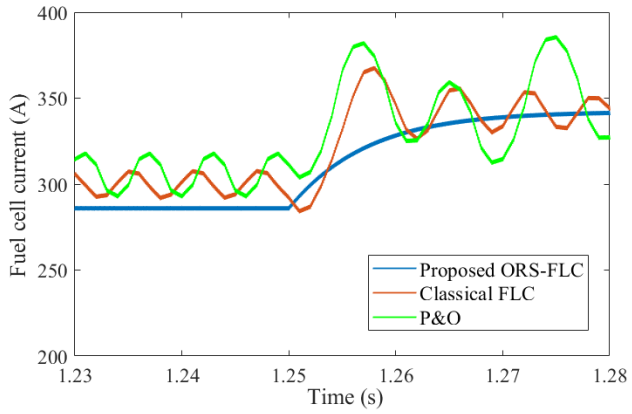

(c) The PEMFC output current.

FIGURE 11. Performance comparison of the proposed ORS-FLC scheme at step increase in T.

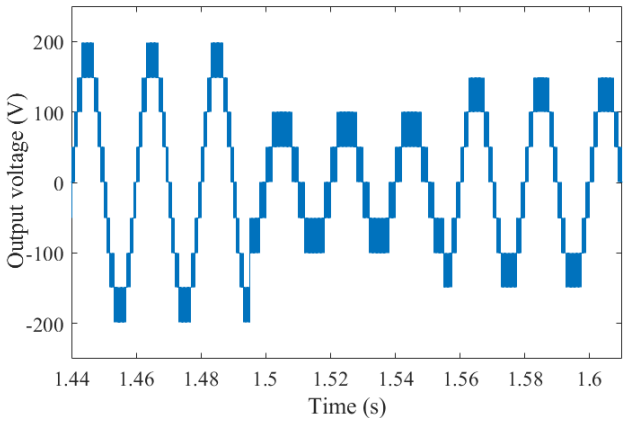

(a) The output voltage.

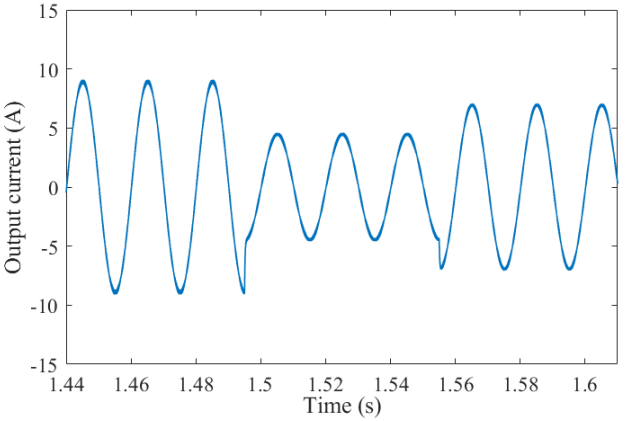

(b) The output current.

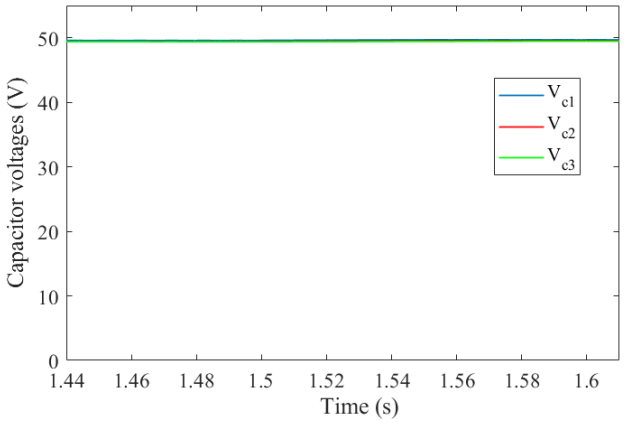

(c) The capacitor voltages.

FIGURE 12. Performance of the proposed high boosting inverter stage at step change in modulation index *mi*.

Fig. 11 shows the comparison between the three methods at step change increase in T from 323 K to 343 K at time 1.25s and constant λ_m of 13. The performance of output power extraction is compared in Fig. 11a between the three studied methods. Although the three methods can track the MPP according to the changes in T, they are different regarding the power ripples and oscillations. The proposed method has the best performance among the three methods. Moreover, the output voltage and current are compared between the three methods in Fig. 11b and Fig.11c, respectively. It can be seen that the proposed method has better terminal voltage waveform than the other studied methods. In addition, the P&O and classical FLC methods have high overshoot values in the output current, which have been effectively eliminated by the proposed ORS-FLC MPPT method.

In this part, the performance of the high boosting factor DC/AC inverter is investigated in Fig. 12. The inverter is tested with step changes in the modulation index *mi* equals

TABLE 4. Comparison of various criteria among existing MPPT schemes.

Criteria	MPPT Methodology				
	P&O	IC/IR	Classical FLC	Optimized FLC	Proposed ORS-FLC
Reference	Ref. [9]	Ref. [8] and Ref. [13]	Ref. [25] and Ref. [26]	Ref. [7]	Proposed
Step Size	Fixed Step	Variable Step	Variable Step	Variable Step	Variable Step
Flexibility	Very Low	Very Low	Medium	Very High	Very High
Design Type	Not Optimum	Not Optimum	Not Optimum	Optimum	Optimum
Output Waveform Fluctuations	High	High	Medium	Small	Very Small
Time of Tracking	High	Very High	Medium	Small	Very Small
No. of sensors	2	2	2	2	1

to 0.9 at starting, *mi* equals to 0.45 at time 1.495s, and *mi* equals to 0.7 at time 1.555s. The output voltage waveform of the inverter is shown in Fig. 12a. It can be seen that, the number of output levels is dependent on the modulation index. In addition, the battery voltage of 50 V has been boosted to 4 times using the proposed topology with having nine levels output voltage. The output voltage can have nine-levels, five-level, and seven-levels at *mi* values of 0.9, 0.45, and 0.7, respectively. The performance of the output current at the three cases is shown in Fig. 12b. It is obvious that the output current is sinusoidal with small ripples at the three cases. Additionally, the capacitor voltages are shown in Fig. 12c. One main advantage of the proposed DC/AC inverter stage is the self-balance capability of the topology without sensing the capacitor voltages. It can be seen that the capacitor voltages remain balanced regardless of the modulation index value. The balance is achieved through the PWM method through charging the capacitors by parallel connection of the three capacitors with the battery.

Table 4 shows comparison of various criteria among the proposed ORS-FLC MPPT method and other methodologies. From the step size point-of-view, they can be classified into: (i) Fixed step type as in the P&O scheme, and (ii) Variable step type as in the IC, IR, classical FLC, optimized FLC, and proposed ORS-FLC methods. Regarding the flexibility, it is evaluated based on the freedom to design the scheme. In P&O method, the only existing flexibility is the selection of suitable step size, which is often compromising the transients with steady state responses. Thence, the flexibility of P&O is very low, which is the same for IC/IR methods. From another side, classical FLC possesses higher flexibility than P&O, and IC/IR methods due to the existing freedom in designing the boundaries of FLC. The optimized FLC version and also the proposed ORS-FLC method increase the flexibility of FLC due to the ability to optimize various parts of FLC. This can be achieved through optimum design of FLC in the proposed ORS-FLC and optimized FLC methods compared with other existing methods. The fluctuations in the output waveforms and speed of tracking have become obvious in the aforementioned obtained simulation results. Furthermore, the proposed ORS-FLC method utilizes reduced number of sensors using only the current measurements compared to the traditionally used two sensors in the other existing methods.

VIII. CONCLUSION

An optimized reduced sensor FLC (ORS-FLC) method is proposed in this article for MPPT control in PEMFC applications. The proposed method solves the problem of tracking optimum operating point of PEMFCs with reduced number of sensors and hence reduced cost of the PEMFC system. Furthermore, a new practical application for the recently developed marine predators algorithm (MPA) for optimizing the design flexibility of the proposed ORS-FLC method. The combination of MPA with proposed ORS-FLC method enables the improved design and selection of various parameters of both input and output membership functions of FLC. The obtained results confirm the effective tracking of MPPT at different operating points. In addition, the proposed ORS-FLC method possesses high tracking speed with reduced oscillations in the output waveforms. Moreover, performance criteria comparisons have been introduced in the paper, which show the superior performance of proposed ORS-FLC method compared to classical methods in addition to other FLC MPPT designs.

REFERENCES

[1] M. M. Alhaider, E. M. Ahmed, M. Aly, H. A. Serhan, E. A. Mohamed, and Z. M. Ali, "New temperature-compensated multi-step constant-current charging method for reliable operation of battery energy storage systems," *IEEE Access*, vol. 8, pp. 27961–27972, 2020.

[2] E. A. Mohamed, E. M. Ahmed, A. Elmelegi, M. Aly, O. Elbaksawi, and A.-A.-A. Mohamed, "An optimized hybrid fractional order controller for frequency regulation in multi-area power systems," *IEEE Access*, vol. 8, pp. 213899–213915, 2020.

[3] S. M. Said, M. Aly, and H. Balint, "An efficient reactive power dispatch method for hybrid photovoltaic and superconducting magnetic energy storage inverters in utility grids," *IEEE Access*, vol. 8, pp. 183708–183721, 2020.

[4] T. Wang, Q. Li, Y. Qiu, L. Yin, L. Liu, and W. Chen, "Efficiency extreme point tracking strategy based on FFRLS online identification for PEMFC system," *IEEE Trans. Energy Convers.*, vol. 34, no. 2, pp. 952–963, Jun. 2019.

[5] C. A. Ramos-Paja, A. Romero, E. Vidal-Idiarte, R. Giral, and L. Martinez-Salamero, "Fuzzy-based modelling technique for PEMFC electrical power generation systems emulation," *IET Power Electron.*, vol. 2, no. 3, pp. 241–255, May 2009.

[6] Z. Qi, J. Tang, J. Pei, and L. Shan, "Fractional controller design of a DC-DC converter for PEMFC," *IEEE Access*, vol. 8, pp. 120134–120144, 2020.

[7] M. Aly and H. Rezk, "A differential evolution-based optimized fuzzy logic MPPT method for enhancing the maximum power extraction of proton exchange membrane fuel cells," *IEEE Access*, vol. 8, pp. 172219–172232, 2020.

[8] A. P. Mohamed, K. R. M. V. Chandrakala, and S. Saravanan, "Comparative study of maximum power point tracking techniques for fuel cell powered electric vehicle," in *Proc. IOP Conf. Ser., Mater. Sci. Eng.*, vol. 577, Dec. 2019, Art. no. 012031.

[9] N. Benyahia, H. Denoun, A. Badji, M. Zaouia, T. Rekioua, N. Benamrouche, and D. Rekioua, "MPPT controller for an interleaved boost DC–DC converter used in fuel cell electric vehicles," *Int. J. Hydrogen Energy*, vol. 39, no. 27, pp. 15196–15205, Sep. 2014.
[10] H. Rezk and A. Fathy, "Performance improvement of PEM fuel cell using variable step-size incremental resistance MPPT technique," *Sustainability*, vol. 12, no. 14, p. 5601, Jul. 2020.
[11] P.-Y. Chen, K.-N. Yu, H.-T. Yau, J.-T. Li, and C.-K. Liao, "A novel variable step size fractional order incremental conductance algorithm to maximize power tracking of fuel cells," *Appl. Math. Model.*, vol. 45, pp. 1067–1075, May 2017.
[12] E. M. Ahmed and M. Shoyama, "Variable step size maximum power point tracker using a single variable for stand-alone battery storage PV systems," *J. Power Electron.*, vol. 11, no. 2, pp. 218–227, Mar. 2011.
[13] A. Harrag and S. Messalti, "Variable step size IC MPPT controller for PEMFC power system improving static and dynamic performances," *Fuel Cells*, vol. 17, no. 6, pp. 816–824, Nov. 2017.
[14] A. Fathy, M. A. Abdelkareem, A. G. Olabi, and H. Rezk, "A novel strategy based on salp swarm algorithm for extracting the maximum power of proton exchange membrane fuel cell," *Int. J. Hydrogen Energy*, vol. 46, no. 8, pp. 6087–6099, Jan. 2021.
[15] K. P. S. Rana, V. Kumar, N. Sehgal, and S. George, "A novel dPdI feedback based control scheme using GWO tuned PID controller for efficient MPPT of PEM fuel cell," *ISA Trans.*, vol. 93, pp. 312–324, Oct. 2019.
[16] Shashikant and B. Shaw, "Comparison of SCA-optimized PID and P&O-based MPPT for an off-grid fuel cell system," in *Soft Computing in Data Analytics*. Singapore: Springer, Aug. 2018, pp. 51–58.
[17] S. Kumar and B. Shaw, "Design of off-grid fuel cell by implementing ALO optimized PID-based MPPT controller," in *Soft Computing in Data Analytics*. Singapore: Springer, Aug. 2018, pp. 83–93.
[18] I. N. Avanaki and M. Sarvi, "A new maximum power point tracking method for PEM fuel cells based on water cycle algorithm," *J. Renew. Energy Environ.*, vol. 3, no. 1, pp. 35–42, Feb. 2016.
[19] M. Inci and A. Caliskan, "Performance enhancement of energy extraction capability for fuel cell implementations with improved cuckoo search algorithm," *Int. J. Hydrogen Energy*, vol. 45, no. 19, pp. 11309–11320, Apr. 2020.
[20] K. Jyotheeswara Reddy and N. Sudhakar, "High voltage gain interleaved boost converter with neural network based MPPT controller for fuel cell based electric vehicle applications," *IEEE Access*, vol. 6, pp. 3899–3908, 2018.
[21] A. Harrag and H. Bahri, "Novel neural network IC-based variable step size fuel cell MPPT controller," *Int. J. Hydrogen Energy*, vol. 42, no. 5, pp. 3549–3563, Feb. 2017.
[22] A. Raj and P. Lekhaj, "An ANFIS based MPPT controller for fuel cell powered induction motor drive," in *Proc. Int. Conf. Smart Grid Clean Energy Technol. (ICSGCE)*, May 2018, pp. 201–205.
[23] S. Ahmadi, S. Abdi, and M. Kakavand, "Maximum power point tracking of a proton exchange membrane fuel cell system using PSO-PID controller," *Int. J. Hydrogen Energy*, vol. 42, no. 32, pp. 20430–20443, Aug. 2017.
[24] Z.-D. Zhong, H.-B. Huo, X.-J. Zhu, G.-Y. Cao, and Y. Ren, "Adaptive maximum power point tracking control of fuel cell power plants," *J. Power Sources*, vol. 176, no. 1, pp. 259–269, Jan. 2008.
[25] H. Rezk, M. Aly, M. Al-Dhaifallah, and M. Shoyama, "Design and hardware implementation of new adaptive fuzzy logic-based MPPT control method for photovoltaic applications," *IEEE Access*, vol. 7, pp. 106427–106438, 2019.
[26] S. D. Al-Majidi, M. F. Abbod, and H. S. Al-Raweshidy, "A novel maximum power point tracking technique based on fuzzy logic for photovoltaic systems," *Int. J. Hydrogen Energy*, vol. 43, no. 31, pp. 14158–14171, Aug. 2018.
[27] A. Harrag and S. Messalti, "How fuzzy logic can improve PEM fuel cell MPPT performances?" *Int. J. Hydrogen Energy*, vol. 43, no. 1, pp. 537–550, Jan. 2018.
[28] N. Harrabi, M. Souissi, A. Aitouche, and M. Chaabane, "Modeling and control of photovoltaic and fuel cell based alternative power systems," *Int. J. Hydrogen Energy*, vol. 43, no. 25, pp. 11442–11451, Jun. 2018.
[29] S. Farajdadian and S. M. H. Hosseini, "Optimization of fuzzy-based MPPT controller via Metaheuristic techniques for stand-alone PV systems," *Int. J. Hydrogen Energy*, vol. 44, no. 47, pp. 25457–25472, Oct. 2019.
[30] P. Bayat and A. Baghramian, "A novel self-tuning type-2 fuzzy maximum power point tracking technique for efficiency enhancement of fuel cell based battery chargers," *Int. J. Hydrogen Energy*, vol. 45, no. 43, pp. 23275–23293, Sep. 2020.
[31] Y. Li, S. Samad, F. W. Ahmed, S. S. Abdulkareem, S. Hao, and A. Rezvani, "Analysis and enhancement of PV efficiency with hybrid MSFLA–FLC MPPT method under different environmental conditions," *J. Cleaner Prod.*, vol. 271, Oct. 2020, Art. no. 122195.
[32] X. Ge, F. W. Ahmed, A. Rezvani, N. Aljojo, S. Samad, and L. K. Foong, "Implementation of a novel hybrid BAT-fuzzy controller based MPPT for grid-connected PV-battery system," *Control Eng. Pract.*, vol. 98, May 2020, Art. no. 104380.
[33] N. Priyadarshi, A. K. Sharma, and F. Azam, "A hybrid firefly-asymmetrical fuzzy logic controller based MPPT for PV-wind-fuel grid integration," *Int. J. Renew. Energy Res.*, vol. 7, pp. 1546–1560, Dec. 2017.
[34] V. Das, S. Padmanaban, K. Venkitusamy, R. Selvamuthukumaran, F. Blaabjerg, and P. Siano, "Recent advances and challenges of fuel cell based power system architectures and control—A review," *Renew. Sustain. Energy Rev.*, vol. 73, pp. 10–18, Jun. 2017.
[35] P. Thounthong, P. Mungporn, D. Guilbert, N. Takorabet, S. Pierfederici, B. Nahid-Mobarakeh, Y. Hu, N. Bizon, Y. Huangfu, and P. Kumam, "Design and control of multiphase interleaved boost converters-based on differential flatness theory for PEM fuel cell multi-stack applications," *Int. J. Electr. Power Energy Syst.*, vol. 124, Jan. 2021, Art. no. 106346.
[36] K. J. Reddy and N. Sudhakar, "ANFIS-MPPT control algorithm for a PEMFC system used in electric vehicle applications," *Int. J. Hydrogen Energy*, vol. 44, no. 29, pp. 15355–15369, Jun. 2019.
[37] Y. Wu, Y. Huangfu, R. Ma, A. Ravey, and D. Chrenko, "A strong robust DC-DC converter of all-digital high-order sliding mode control for fuel cell power applications," *J. Power Sources*, vol. 413, pp. 222–232, Feb. 2019.
[38] J. Chen, C. Wang, and J. Li, "A single-phase step-up seven-level inverter with a simple implementation method for level-shifted modulation schemes," *IEEE Access*, vol. 7, pp. 146552–146565, 2019.
[39] S. S. Lee, "A single-phase single-source 7-level inverter with triple voltage boosting gain," *IEEE Access*, vol. 6, pp. 30005–30011, 2018.
[40] A. Taghvaie, J. Adabi, and M. Rezanejad, "A self-balanced step-up multilevel inverter based on switched-capacitor structure," *IEEE Trans. Power Electron.*, vol. 33, no. 1, pp. 199–209, Jan. 2018.
[41] M. Saeedian, M. E. Adabi, S. M. Hosseini, J. Adabi, and E. Pouresmaeil, "A novel step-up single source multilevel inverter: Topology, operating principle, and modulation," *IEEE Trans. Power Electron.*, vol. 34, no. 4, pp. 3269–3282, Apr. 2019.
[42] Y. Hinago and H. Koizumi, "A switched-capacitor inverter using series/parallel conversion with inductive load," *IEEE Trans. Ind. Electron.*, vol. 59, no. 2, pp. 878–887, Feb. 2012.
[43] A. Faramarzi, M. Heidarinejad, S. Mirjalili, and A. H. Gandomi, "Marine predators algorithm: A nature-inspired metaheuristic," *Expert Syst. Appl.*, vol. 152, Aug. 2020, Art. no. 113377.

MOKHTAR ALY (Member, IEEE) received the B.Sc. and M.Sc. degrees in electrical engineering from Aswan University, Aswan, Egypt, in 2007 and 2012, respectively, and the Ph.D. degree from the Department of Electrical Engineering, Faculty of Information Science and Electrical Engineering, Kyushu University, Japan, in 2017.

In 2008, he joined the Department of Electrical Engineering, Aswan University, as an Assistant Lecturer, where he has been an Assistant Professor with the Faculty of Engineering, since 2017. He is currently a Postdoctoral Researcher with the Solar Energy Research Center (SERC-Chile), Universidad Técnica Federico Santa María, Chile. His current research interests include reliability of power electronics systems especially in renewable energy applications, multi-level inverters, fault tolerant control, electric vehicles, and light emitting diode (LED) lamp drivers. He is a member of the IEEE Power Electronics Society (PELS), the IEEE Industrial Electronics Society (IES), and the IEEE Power and Energy Society (PES).

EMAD M. AHMED (Senior Member, IEEE) received the B.Sc. and M.Sc. degrees from Aswan University, Egypt, in 2001 and 2006, respectively, and the Ph.D. degree from Kyushu University, Japan, in 2012.

He was a member of the Aswan Power Electronics Applications Research Center (APEARC), from 2012 to 2018. In 2018, he joined the Aswan Wireless Communication Research Center (AWCRC). He is currently working as an Associate Professor with the Department of Electrical Engineering, Faculty of Engineering, Aswan University. He is on a leave at the Faculty of Engineering, Jouf University, Saudi Arabia. His current research interests include applied power electronics, especially in renewable energy applications, micro-grids, fault tolerant control, and battery management systems. He is a member of the IEEE Power Electronics Society (PELS), the IEEE Industrial Electronics Society (IES), and the IEEE Power and Energy Society (PES).

HEGAZY REZK received the B.Eng. and M.Eng. degrees in electrical engineering from Minia University, Egypt, in 2001 and 2006, respectively, and the Ph.D. degree from the Moscow Power Engineering Institute, Moscow. He was a Postdoctoral Research Fellow with the Moscow State University of Mechanical Engineering, in 2014. He was a Visiting Researcher with Kyushu University, Japan, in 2015. He is currently an Associate Professor with the Electrical Engineering Department, College of Engineering at Wadi Addwaser, Prince Sattam University, Saudi Arabia. He has authored more than 100 technical articles. His current research interests include renewable and sustainable energy, energy management, energy efficiency modern optimization algorithms, and modeling based on artificial intelligence.

EMAD A. MOHAMED received the B.Sc. and M.Sc. degrees in electrical power engineering from Aswan University, Aswan, Egypt, in 2005 and 2013, respectively, and the Ph.D. degree in electrical power engineering from the Kyushu Institute of Technology, Japan, in 2019.

He was a Demonstrator with the Department of Electrical Engineering, Aswan Faculty of Engineering, Aswan University, from November 2007 to August 2013, and an Assistant Lecturer from 2013 to 2015. He was a Research Student with Kyushu University, Japan, from April 2015 to October 2015. He has been an Assistant Professor since May 2019. He was with the Faculté des Sciences et Technologies, Université de Lorraine, France–1, with the Master Mobility Scholarship. The scholarship sponsored by FFEEBB ERASMUS MUNDUS. His current research interests include applications of superconducting power devices, power system stability, and reliability and protection.